Molecular Physics

An International Journal at the Interface Between Chemistry and Physics

ISSN: (Print) (Online) Journal homepage: https://www.tandfonline.com/loi/tmph20

Ion molecule reaction dynamics for disentangling competing reactive pathways

Marcel Meta & Jennifer Meyer

To cite this article: Marcel Meta & Jennifer Meyer (09 Jan 2024): Ion molecule reaction dynamics for disentangling competing reactive pathways, Molecular Physics, DOI: 10.1080/00268976.2023.2293228

To link to this article: https://doi.org/10.1080/00268976.2023.2293228

Published online: 09 Jan 2024.

MOLECULAR PHYSICS e2293228
https://doi.org/10.1080/00268976.2023.2293228

Taylor & Francis
Taylor & Francis Group

RESEARCH ARTICLE

OPEN ACCESS Check for updates

Ion molecule reaction dynamics for disentangling competing reactive pathways

Marcel Meta and Jennifer Meyer

Fachbereich Chemie und Landesforschungszentrum OPTIMAS, RPTU Kaiserslautern-Landau, Kaiserslautern, Germany

ABSTRACT

Chemical reactions are by definition dynamical. Reactants move towards each other, collide and products separate again. Therefore, it is important to look beyond the stationary description, and look at how molecules rearrange and how energy is partitioned during a reactive collision. Chemical reactions are complex and often involve competing chemical and/or atomistic pathways whose dominance depends on several factors as for example the involved quantum states or collision energy. Here, we focus on ion molecule reactions which play an important role in gaseous environments even though their steady-state abundance is often much lower than that of their neutral counterparts. We present the use of angle and energy differential cross sections from crossed beam imaging experiments to disentangle competing reaction pathways. The general term pathways includes different effects of specific reactant quantum states on the atomistic mechanism to the competition of different product channels.

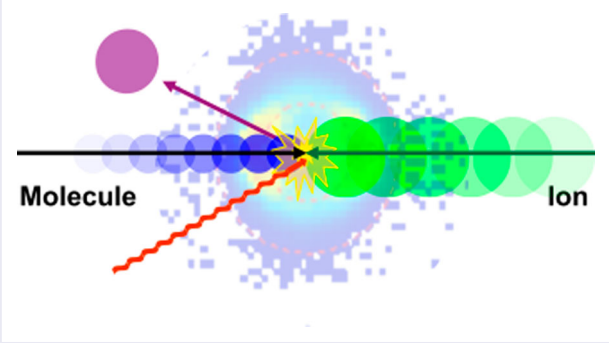

ARTICLE HISTORY
Received 20 October 2023
Accepted 4 December 2023

KEYWORDS
Gas phase; ion molecule reaction dynamics; crossed beam velocity map imaging; polyatomic; quantum states

1. Introduction

The interaction of an energetic particle or photon with a molecule can lead to ion formation. Gas phase ion molecule reactions are characterised by much larger collision cross sections compared to their neutral-neutral counterpart [1] due to the attractive long-range interactions based on the ion's charge and the polarisability, dipole or quadrupole moment of the neutral molecule. This makes ion molecule reactions important constituents of chemical networks in atmospheric models or the interstellar medium even though their much lower steady-state abundance compared to neutral molecules might not suggest it at first glance [2–5]. While for the modelling of molecular abundances by chemical networks rate constants, or integral cross sections, are important, we aim at the dynamics of the reaction. We focus on how the product is formed, which we refer to as reaction dynamics. The main objective of molecular reaction dynamics is to understand how a chemical reaction happens between two reactants at the molecular level, i.e. how atoms rearrange and how energy is partitioned during the reactive collision. The basic concepts of collisions between hard spheres dates back to nineteenth century [6] but we still apply the general line of arguments in classic collision theory today albeit with more sophisticated models for the attractive long-range interactions [7]. Even though the concepts were developed for elastic collisions, we generally also apply them to reactive collisions if the scattering length is much larger than the molecular dimensions. The angle and energy differential

CONTACT Jennifer Meyer jennifer.meyer@chem.rptu.de Fachbereich Chemie und Landesforschungszentrum OPTIMAS, RPTU Kaiserslautern-Landau, Erwin-Schrödinger-Straße 52, Kaiserslautern 67663, Germany

cross section, i.e. product flux as a function of product energy and scattering angle, is sensitive to the interaction potential between the particles [8,9]. We correlate the scattering angle, i.e. the deflection of our product, to a collision geometry of the interacting molecules. In general, large impact parameter collisions lead to little momentum transfer while small impact parameters lead to large momentum transfer up to the limiting case of so-called head-on collisions associated with momentum reversal. Reactions upon impact are termed direct [10]. If the reactants form an interaction complex whose lifetime exceeds several rotational periods, information about the initial collision geometry is lost and subsequent statistical decay leads to isotropic scattering [10]. We can deduce the atomistic mechanisms leading to product formation from the experimental differential cross sections taking energy and momentum (linear and angular) conservation into account [8–12]. A typical gas phase ion molecule reaction coordinate is characterised by a transition state with deep potentials wells to either side which are often referred to as pre-reaction and post-reaction wells or entrance and exit wells (see Figure 1). According to statistical arguments, a transition state which is submerged relative to the free reactants should exert no (measurable) influence on the reaction kinetics. However, it is known that especially for gas phase reactions involving few atoms, non-statistical effects occur [13]. The most prominent examples are the so-called Polanyi rules which compare the influence of vibrational and translational excitation on a reaction [12]. Energetic resonances and (stereo)dynamic constraints may lead to such non-statistical effects even for exothermic reactions for which barriers are all submerged with respect to the entrance channel [13]. Differential cross sections under single collision conditions are therefore an essential tool to experimentally probe these phenomena with the ultimate aim of state-to-state scattering experiments.

In chemical reactions, competitions between different product channels are a common phenomenon. Competing channels may form the same product but by different atomistic mechanisms, in different final states or altogether distinct product species may be formed. Three important input parameters of any reactive scattering experiment are (1) the accessible collision energies, (2) the chemical complexity and (3) the desired quantum state resolution. However, one has to be aware that the three parameters are not entirely independent of each other. For example, in diatom-atom collisions, we can achieve a higher degree of quantum state control than in polyatomic reactions because of fewer ro-vibrational states which can be populated in reactants as well as products. Considering the first parameter listed above, the relative collision energy, current

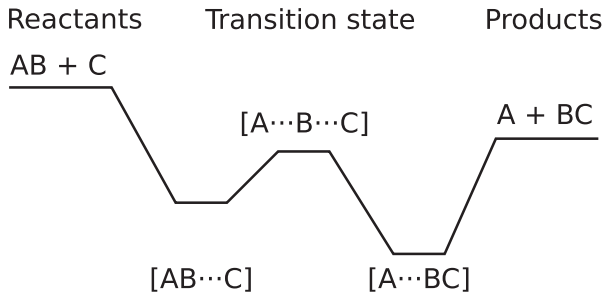

Figure 1. Schematic of a reaction coordinate for an exothermic gas phase reaction. *A*, *B* and *C* are place holders and can represent a single atom as well as a complex molecule. [AB··· C] represents the interaction between the reactants within the pre-reaction well and [A··· BC] that within the post-reaction well after the products are formed.

experiments can be loosely associated with two regimes: Low energy and ultracold collisions. Ultracold collisions probe chemistry down to collision energies in the milli-Kelvin regime using for example either merged beam techniques [14–16] or ion trapping techniques [17–20]. While these experiments offer a high level of control over the state distributions of the reactant, they are currently either limited to very small systems (merged beams) or not able to easily probe scattering angle distributions (ion traps). Here, we want to focus on experiments directly probing the differential cross sections in the low collision energy regime, that is commonly associated to collisions with up to 5 eV collisions. Several experimental set-ups for low energy reactive ion molecule scattering have been developed over the years [21–27] and developments in ion molecule reactive crossed beam scattering experiments have been recently reviewed [28–30]. The present review highlights four ion molecule reactive scattering experiments [27,31–38] that focus on disentangling competing pathways by the combination of crossed beams with velocity map imaging [39]. In general, a crossed beam set-up for reactive scattering combines an ion source, a molecular beam source and the velocity map imaging spectrometer including a time and position sensitive detector. Ion sources and the electrostatic lens stack of the spectrometers are designed according to the objectives of the respective experiment, i.e. target species, reactant quantum state distribution, collision energy and desired energy resolution as well as interaction volume. Product ions are mapped onto a position and time sensitive detector to record the product ion velocity distributions, ideally in all three dimensions to recover the 3D Newton sphere which has been crunched onto the 2D detector in the course of the mapping. Converting the crunched Newton sphere back to three dimensions can either be achieved by simultaneously recording an ion's

time-of-flight to recover v_z [40] or by an instrument function [24]. Alternatively, one can record only the central slice of the 3D distribution [41]. Recently, new instruments have been developed with the goal of quantum state-to-state scattering [26,42,43]. These take up the original approach of Weisshaar [21] to prepare ions state-selectively by photoionisation. While Weisshaar and co-workers photoionised within the interaction region, the new experiments use external ion sources and transfer the ions into the interaction region like the instruments developed by the Wester [22] and Farrar [24] groups. Wester and co-workers have gone one step further by planning a coincidence experiment to reduce the experimental uncertainty of the product velocity distribution by measuring the exact center-of-mass for each collision event using both product velocities measured in coincidence [43].

In the following, we will increase the chemical complexity as we move from atom-diatom reactions ($Ar^+ + N_2$) to poly-atomic reactions (e.g. $F^- + (CH_3)_3CCl$). Together with the involved number of atoms, the complexity of respective reaction mechanisms increases from charge transfer to base-induced elimination where the simultaneous formation and breaking of several chemical bonds happens. At the same time, the question about the importance of quantum state population on the dynamics is raised.

2. (Di)Atom-diatom reactions

Since the pioneering days of molecular reaction dynamics [10,11,44], technological and scientific progress opened up new possibilities. Still, the evaluation of state-to-state differential cross sections requires the precise knowledge of all degrees of freedom of a system. Here, we want to focus on recent progress towards state-to-state scattering for ion molecule reactions. $Ar^+ + N_2$ is well-studied but the impact of the spin-orbit state of Ar^+ has left open questions. Reactions involving several spin states are ubiquitous in transition metal ion molecule reactions, which is referred to as multi-state or in special cases as two-state reactivity [45]. Understanding the influence of intersystem crossing on the dynamics is an open question in neutral-neutral scattering [46] as well as for ion-molecule reactions [27]. The two presented systems are chemically very different from each other, however, they have in common that both ions are open-shell, i.e. have unpaired electrons and consequently are highly reactive species. They both have close lying electronic states and (might) show vastly different chemistry, i.e. reactivity and possibly dynamics as function of the electronic state, respectively the electron configuration.

2.1. State-to-state dynamics for $Ar^+ + N_2$

The transfer of an electron is a conceptually simple reaction because no bond cleavage or formation is involved. However, charge transfer reactions are intrinsically non-adiabatic often involving multiple electronic surfaces leading to a break-down of the Born-Oppenheimer approximation. Here, we want to concentrate on a very specific charge transfer reaction: $Ar^+ + N_2$ [25,31,47–53].

$$Ar^+(^2P_J) + N_2(^1\Sigma_g^+, v = 0) \rightarrow Ar(^1S_0) + N_2^+(^2\Sigma_g, v') \quad (1)$$

The reaction has drawn attention over the years due to the fact that the reaction yields N_2^+ in $v = 1$ as main product channel. The channel is endothermic by 92 meV but near resonant with Ar^+ in its $^2P_{3/2}$ state. Experiments found different scattering signatures and did not agree on the degree of ro-vibrational excitation of the N_2^+. The reactivity is dominated by the accessibility and efficiency of curve crossings and no crossing exists for the ground vibrational state of N_2^+ [49,54].

Reactive scattering experiments at low relative collision energies ($E_{rel} < 2$ eV) measured the differential cross section probing the reaction on the electronic ground state using a combination of crossed beams with velocity map imaging [53,55]. The N_2^+ velocity distribution is dominated by forward scattering into small scattering angles. This is in-line with the general concept of charge transfer reactions already happening at large distances, i.e. large reactive impact parameters associated with minimal momentum transfer. Upon closer inspection, it became obvious that some product ions are scattered into higher angles. These lower impact parameter collisions lead to higher ro-vibrational excitation of the N_2^+ [53]. The authors derive up to six quanta of vibrational excitation of the N_2^+ with additional 60 meV in rotational degrees of freedom. However, they did not find evidence of a scattering resonance around 1 eV collision energy seen in earlier experiments as backward scattering signature [48]. Their ratio of N_2^+ ions in $v' = 1$ to those in $v' = 2$ is lower than predicted [49] while reproducing the general trend. The influence of the spin-orbit state of the Ar^+ remained elusive. The argon ions were formed in a plasma discharge source by electron impact ionisation and a statistical distribution of spin orbit states was assumed. Recent photo dissociation experiments of $[Ar - N_2]^+$ found the vibrational state of N_2^+ to be correlated to the spin-orbit state of the Ar^+ [56] with the non-adiabatic pathway being much more pronounced in case of Ar^+ ($^2P_{3/2}$) compared to Ar^+ ($^2P_{1/2}$). Overall experimental and theoretical results suggest not only a state specific reactivity but also state specific dynamics.

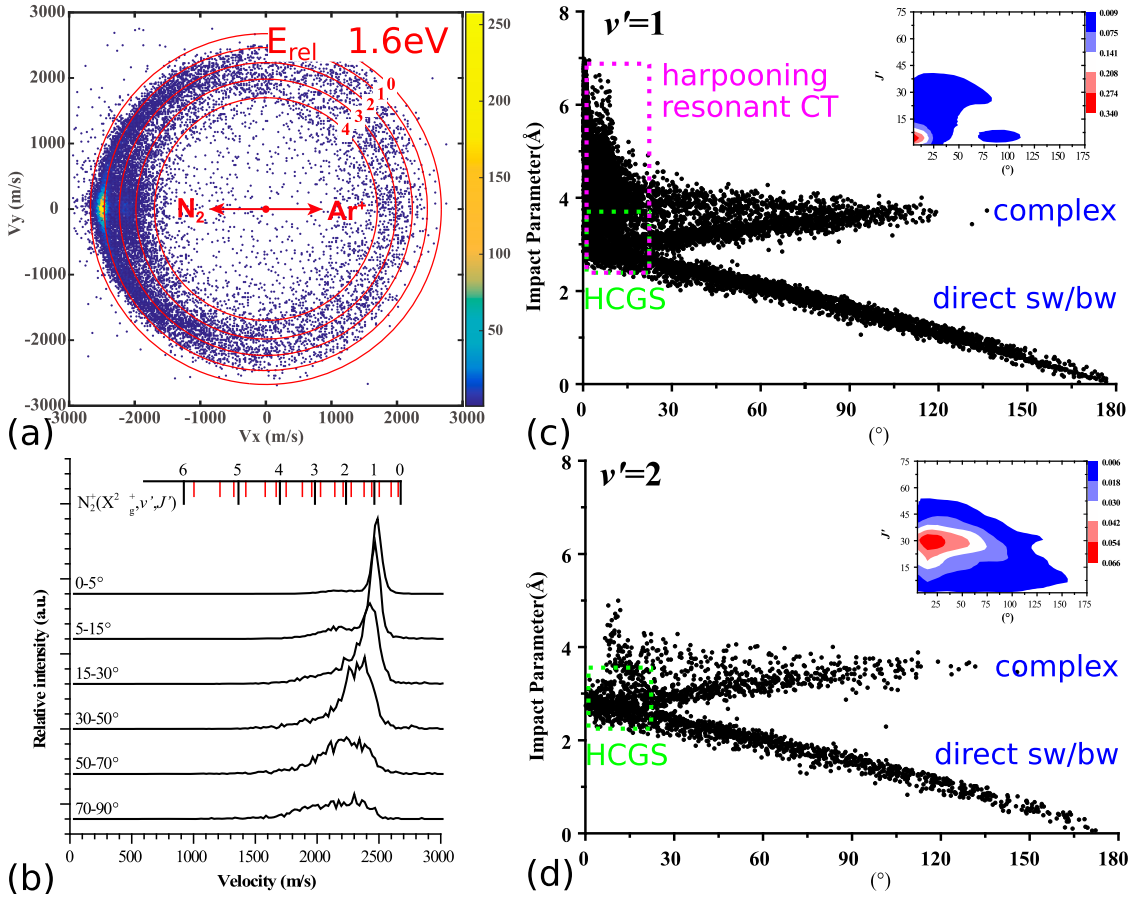

Figure 2. (a) Central slice of the 3D velocity distribution for the reaction $Ar^+(P_{3/2}) + N_2(v = 0) \rightarrow Ar + N_2^+(v')$ at a relative collision energy of $\approx$ 1.6 eV. Red arrows indicate the collision geometry and red rings give the kinematic cut-off for different final vibrational states of N_2^+. The kinematic cut-off gives the maximum possible product ion velocity considering energy and momentum conservation. (b) Velocity integrated distributions for different angular cuts of the scattering distribution with rotational (red) and vibrational (black) levels given as drop lines. (c) and (d) show the correlation between the reactive impact parameter and the scattering angle for N_2^+ in (c) $v' = 1$ and (d) $v' = 2$ from surface hopping calculations. The insets show the respective rotational state distributions as function of scattering angle. Scattering ranges for different atomistic mechanisms are indicated. Figure adapted with permission from [31], copyright 2023 by SpringerNature.

Recently, Gao *et al.* commissioned a new crossed beam experiment in which they use a photoionisation scheme to selectively form Ar^+ in its $^2P_{3/2}$ state [31]. Their results are in general agreement with those of Wester *et al.* [53,55] but the state specificity allows them deeper insight into the ro-vibrational state distribution of N_2^+ (see Figure 2). They find that N_2^+ scattered into higher angles is not dominated by vibrational but rotational excitation [31]. Further, the energy partitioning differs for N_2^+ in $v' = 1$ and $v' = 2$ with $v' = 2$ showing much higher rotational excitation than $v' = 1$. The differential cross section for $v' = 1$ is dominated by the large impact parameter resonant charge transfer with some contribution from low impact parameters, which lead to near isotropic scattering features (see Figure 2(c,d)). For $v' = 2$, on the other hand, the small impact parameter collisions significantly contribute to forward scattered N_2^+ with the rotational population peaking around $J = 30$. Rotational populations and impact parameter dependence of the scattering angle are obtained from theory using surface hopping [31,57]. Gao *et al.* attribute the small impact parameter forward scattering mechanism to *hard collision glory scattering* (HCGS), which has been seen in inelastic scattering experiments [58] but not yet been assigned in reactive scattering. The forward scattering is surprising because in hard sphere collision theory, small impact parameters lead to backward scattering. However, the $Ar^+ + N_2$ interaction potential has a relatively strong attraction at short distances which partially counters the repulsive part and leads in summary to forward scattering associated with relatively high rotational excitation. A picture one can envision is the N_2^+ being scattered sideways, respectively backwards, by the repulsive part of the potential and immediately caught by an attractive interaction steering the particle into a forward directed motion [31,58,59].

2.2. Transition metal ion molecule reactions

Crossed beam imaging experiments of transition metal ion molecule reactions are rare. On the one hand, they pose a challenge to experimentalist to reliably produce ions in sufficiently high numbers for scattering experiments and on the other hand to quantum chemistry regarding the often high number of close lying electronic states found for transition metal ions.

One rare example is the reaction between Co^+ and propane (C_3H_8) by the Weisshaar group in the early 2000s [21]. They investigated the angle and energy differential cross section at a relative collision energy of about 0.2 eV. Two product channels are energetically accessible, namely formation of methane and molecular hydrogen. The formation of methane is about five times more likely than the formation of H_2. The analysis of the angular distribution revealed that the formation of methane tends to produce images with a trend to forward-backward symmetry, whereas the formation of H_2 tends to produce a more isotropic scattering.

New experimental differential cross sections for transition metal ion molecule reactions have not been available until we recently published the first data from our new crossed beam imaging experiment [27]. We studied the oxygen atom transfer reaction between carbon dioxide and the tantalum cation Ta^+, which are four atoms compared to the 12 atoms in the Weisshaar experiment. $Ta^+ + CO_2$ is an already well-studied reaction [60–63] but the experimental data from our group complements the existing data because we recorded energy and angle differential cross sections (see Figure 3a–c). We varied the relative collision energy (1, 1.5, 2.0 eV) to gain insight into the energy partitioning and the potential influences of the intersystem crossing (ISC) on the dynamics.

The green and orange ring in the first row of Figure 3(a) represent the kinematic cut-off for specific states (green ring for $^5Ta^+$ and orange ring for $^3Ta^+$). The kinematic cut-off represents the maximum possible product ion velocity considering energy and momentum conservation in the single collision experiment. The TaO^+ ions are predominantly isotropically scattered around the center-of-mass. The scattering distribution shifts slightly into the forward hemisphere with increasing collision energy. This can be observed in a more quantitative way in the integrated angular distribution in the second column of Figure 3(e–g). The isotropic scattering combined with the low product ion velocities are fingerprints for indirect dynamics where an interaction complex whose lifetime exceeds the rotational period is formed. During the complex' lifetime, energy is efficiently partitioned into internal degrees of freedom leading to low product velocities. The experimental resolution and low product ion velocities well-within the kinematic cut-off of the ground state reaction are the reasons why a direct disentanglement of the individual contributions of the two electronic states of Ta^+ is currently challenging by experiment alone. We, however, have compelling arguments that most the observed reactivity is due to ground state reactants [27]. Insight into the energy partitioning can be gained by looking at the kinetic energy of the product ions TaO^+ as well as the energy channelled into internal degrees of freedom of both molecular products TaO^+ and CO (see Figure 3g). From the comparison, it can be seen that a large part of the available energy is redistributed into internal energy. Furthermore, the additional relative collision energy is also almost exclusively transferred into internal excitation meaning ro-vibrational degrees of TaO^+ and/or CO. This all requires the presence of a bottleneck along the reaction coordinate for this apparently simple four atom reaction which is exothermic by more than 2 eV. For the counter-intuitive forward tendency at higher relative collision energies, it is assumed that a direct rebound mechanism happens which results from near head-on collisions and the resulting large momentum transfer. Based on this observation, a co-linear approach geometry is assumed, which is consistent with the calculated geometric structures of the pre-reaction well, where an oxygen atom of the carbon dioxide points to the tantalum cation.

3. Polyatomic reactions

Progressing from the classic atom-diatom to polyatomic reactions, which are commonly all reactions with more than three atoms, competing pathways for product formation become possible. For these pathways, we may have to consider the number of ro-vibrational states of the reactants as well as reactions leading to entirely different products. The increasing number of possible pathways for the reaction makes the assignment of outcomes to individual inputs ever more challenging.

3.1. Vibrational vs. translational excitation: $F^- + CH_3I$

The dynamics of chemical reactions are sensitive to changes in the interaction potential of the two colliding particles. Besides the intrinsic potential, the question of how the energy partitioning in the reactants affects not only the efficiency but also the dynamics of a reaction has intrigued scientists since the early days of molecular reaction dynamics.

Polanyi linked the efficiency of translation compared to vibrational excitation to promote a reaction to

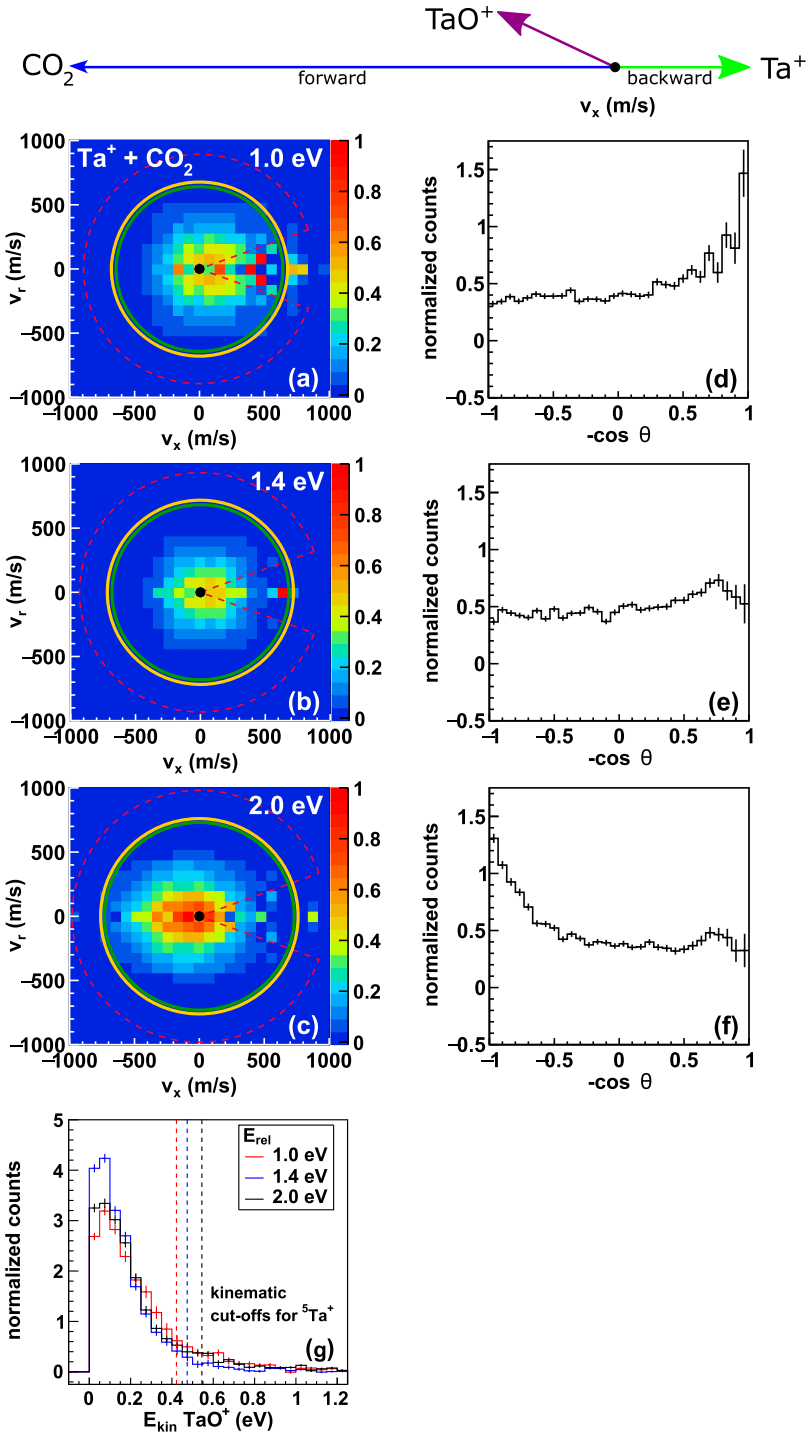

Figure 3. Experimental differential cross sections for $Ta^+ + CO_2$. The first column (panels a–c) shows the velocity distributions of the TaO^+ cation at relative collision energies between 1 and 2 eV. The kinematic cut-off of the electronic ground state ($^5Ta^+$, green) and the first electronically excited state ($^3Ta^+$, orange) are represented by the superimposed circles. They give the maximum possible product ion velocity considering energy and momentum conservation due to the single collision conditions of the experiment. Panel (g) shows a direct comparison of the normalised integrated kinetic energy distributions of TaO^+ for all three collision energies. The second column (panels e–f) shows the integrated angular distributions. The pink line indicates the area integrated to obtain the kinetic energy distribution. All 1D histograms are normalised to unity. Figure adapted from [27].

the location of the transition state along the reaction coordinate. Translation is more efficient to promote a reaction than vibration for a reactant-like transition state and vice versa for a product-like transition state [12]. The so-called Polanyi rules are often used in a broad context, but they were derived for atom-diatom collisions.

Once polyatomic reactants are involved, the number of ro-vibrational states increases, leading to the question if a model developed for atom-diatom reactions is still applicable. Liu and co-workers studied the effect of ro-vibrational excitation in a set of reactions of the type $X + CD_3H$ (X = F, Cl, O) for which they found inhibition as well as enhancement of the overall reactivity as well as effects on the differential cross section when exciting the symmetric CH stretching mode [64,65]. The authors argue that the effects are in part mediated by changes in the long-range interaction potential. These, in turn, lead to changes in the range of reactive impact parameters for a given relative orientation of the reactants with respect to each other. The range of orientations, respectively collision geometries, which lead to a reaction was named cone-of-acceptance [8]. Hence, it is possible for the cone to open, leading to larger reactive impact parameters, or close with the reverse effect. In case of ion molecule reactions, the long-range interaction is dominated by the charge-(induced)dipole interaction, posing the question if such subtle effects can also be observed for ion molecule reactions.

Wester and co-workers set out to experimentally answer the question if excitation of the symmetric CH stretching mode acts as a spectator in a bimolecular nucleophilic substitution S_N2 reaction or not by recording energy and angle differential cross sections for $F^- + CH_3I$ [28,29,66–68] (reaction (2)). Chemical intuition suggests a spectator mode behaviour but conflicting theoretical predictions existed [69]. Further, the first interaction complex between the CH_3I and the F^- is hydrogen-bonded making an influence of the C–H stretching mode conceivable [66].

$$F^- + CH_3I \rightarrow I^- + CH_3F \quad (2)$$

$$\rightarrow CH_2I^- + HF \quad (3)$$

$$\rightarrow FHI^- + CH_2 \quad (4)$$

$$\rightarrow FI^- + CH_3 \quad (5)$$

In the experiment, the relative collision energy was set to the threshold energy of an endothermic proton transfer channel (reaction (3)), such that the collision energy plus one quantum in the symmetric CH stretching mode provided enough total energy for the proton transfer to become accessible [23,70]. The reactivity of the proton transfer is enhanced upon vibrational excitation as chemical intuition suggests, because the CH bond which is vibrationally excited, is the one being broken during the reaction [32]. Therefore, the proton transfer can be used as an *internal standard* to confirm the presence of vibrationally excited CH_3I molecules within the interaction region of the velocity map imaging spectrometer. This was especially important because experiments confirmed the spectator mode behaviour of the symmetric CH stretching mode ν_1 for the S_N2 channel (reaction (2)), that is, the experiment found no changes in the reactivity or dynamics [32]. The spectator mode behaviour was supported by predictions using the Sudden Vector Projection model [32]. The model was developed by Guo and co-workers as a generalisation of Polanyi's rules to polyatomic systems [71]. However, no effect on the dynamics has been observed. In a second set of experiments, the collision energy range and the investigated reaction channels were extended (reactions (4), (5)) [33]. Here, a slight effect on the efficiency of the S_N2 channel has been observed at 2 eV relative collision energy.

While the dynamics of the S_N2 reaction have not changed, the dynamics of the proton transfer reaction is affected by vibrational excitation [34]. The effects observed in the differential cross section are dependent on collision energy but can be traced back to a common effect. At the lower collision energy the angular distribution upon vibrational excitation shifts to a forward-backward symmetric distribution and to forward scattered CH_2I^- by a direct mechanism at higher collision energies (see Figure 4). Both changes are indicators for large impact parameter collisions becoming more prominent. However, the mean elongation of the CH bond due to one quantum in the ν_1 mode does not support the observed pronounced effect. The authors, therefore, speculate that the long-range interaction potential is altered similar to the effects seen by Liu and co-workers for $X + CHD_3$ reactions [65]. They propose a lensing effect, which leads to pre-orientation of the reactants prior to collision and to larger reactive impact parameters.

3.2. Disentangling competing reaction pathways: $F^- + R_3CCl$

One of the most well-known applications of anions is in synthetic chemistry, e.g. in nucleophilic substitution and base-induced elimination [72]. In gas phase, the bimolecular variations can be investigated, i.e. the S_N2 and E2 reactions [68]. The choice of conditions (the nucleophile, the leaving group and the solvent environment) influences the reactivity of both reactions in very similar ways [72]. In S_N2 reactions, the nucleophile attacks the so-called α-carbon centre to which the leaving group is bound. With respect to stereodynamics this leads to a concerted reaction with the so-called Walden inversion [73], i.e. the CR_3 umbrella flips during product formation. On the other hand, base-induced elimination (E2) has two possible routes: syn- and anti-elimination. Syn

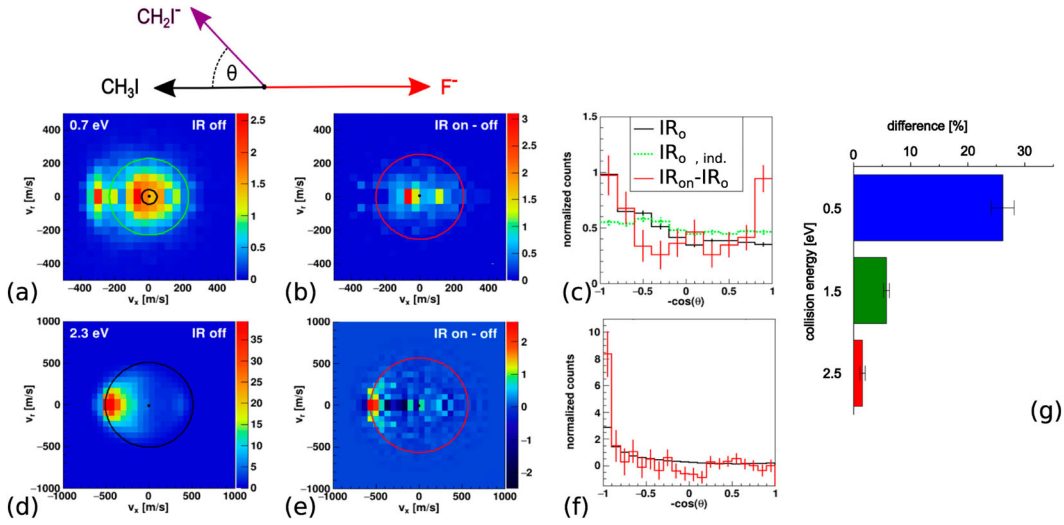

Figure 4. Product ion CH_2I^- velocity distributions for the proton transfer channel for $F^- + CH_3I$. The left column shows the distribution for the ground state reaction (laser off) while the central column shows the distribution for the reaction of vibrationally excited CH_3I (laser off − laser on). The angle-integrated distributions are shown in the right column. The superimposed circles indicate the respective kinematic cut-offs (black $\nu_1 = 0$, red $\nu_1 = 1$). The relative change in reactivity is visualised by the box plots. Adapted from [33,34].

and anti refer to the relative orientation of the attacking base and the leaving group with respect to the carbon backbone of the alkyl halide. If both groups are on the same side of the C–C backbone, it is called syn-elimination and if they are on opposite sites, it is anti-elimination. The parameter to steer the competition between S_N2 and E2 is the steric hindrance at the α-carbon blocking the access of the nucleophile. The challenge for gas phase experiments to disentangle S_N2 and E2 is the fact that both mechanisms form the same ionic product (see for example reactions (7) and (8)). The dynamics, however, are expected to be vastly different.

The Wester group performed various studies to investigate in detail the influence of nucleophile, leaving group and the steric environment at the α-carbon [23,35,37,38,66,74–76]. Here, selected studies will be compared with respect to the steric hindrance at the α-carbon. For three collision energies, differential cross sections of the type $X^- + RY$ (reactions (6)–(10)) are shown in Figure 5 [35–38].

$$F^- + CH_3Cl \rightarrow Cl^- + CH_3F \quad (6)$$

$$F^- + CH_3CH_2Cl \rightarrow Cl^- + CH_3CH_2F \quad (7)$$

$$\rightarrow Cl^- + HF + CH_2CH_2 \quad (8)$$

$$F^- + (CH_3)_3CCl \rightarrow Cl^- + (CH_3)_3CF \quad (9)$$

$$\rightarrow Cl^- + HF + CH_2C(CH_3)_2 \quad (10)$$

Already at low collision energies, the reaction of F^- with methyl chloride CH_3Cl shows direct dynamics as can be seen by ions scattered at high velocities into a backward umbrella [35]. With increasing collision energy the products are being scattered almost exclusively into the backwards hemisphere. These events are related to a direct rebound mechanism, which in chemistry is known as Walden inversion [73]. This observation is even more obvious in the integrated angular distribution (Figure 5(d)). E2 is not possible in the reaction with methyl chloride but it becomes accessible once the carbon backbone constitutes at least two carbon atoms, i.e. for the higher substituted chloro alkanes starting with ethyl chloride CH_3CH_2Cl (here reactions (8) and (10)). In the case of tertiary carbon centres as for *tert*-butyl chloride $(CH_3)_3CCl$, i.e. with none of the three other bonds at the α-carbon being a bond to a hydrogen atom, the substitution reaction is considered fully suppressed due to steric hindrance [72], although this is contested by recent trajectory simulations [77].

In the reaction between *tert*-butyl chloride and F^-, a symmetrical forward-backward scattering signature is observed at low collision energies (Figure 5(l,m)). This scattering signature is associated to large reactive impact parameters which lead to a complex-mediated mechanism whose dissociation plane is confined by angular momentum conservation rules [10]. In addition, a widespread isotropic scattering can be seen, which is independent of the collision energy in the investigated energy range [37]. In contrast, the symmetrically forward-backward scattered products from indirect dynamics are replaced by events scattered into the forward hemisphere by a stripping-like direct mechanism at high collision energies [36,74]. Three collision energy dependent mechanisms and one collision energy independent mechanism have been identified for E2 [37].

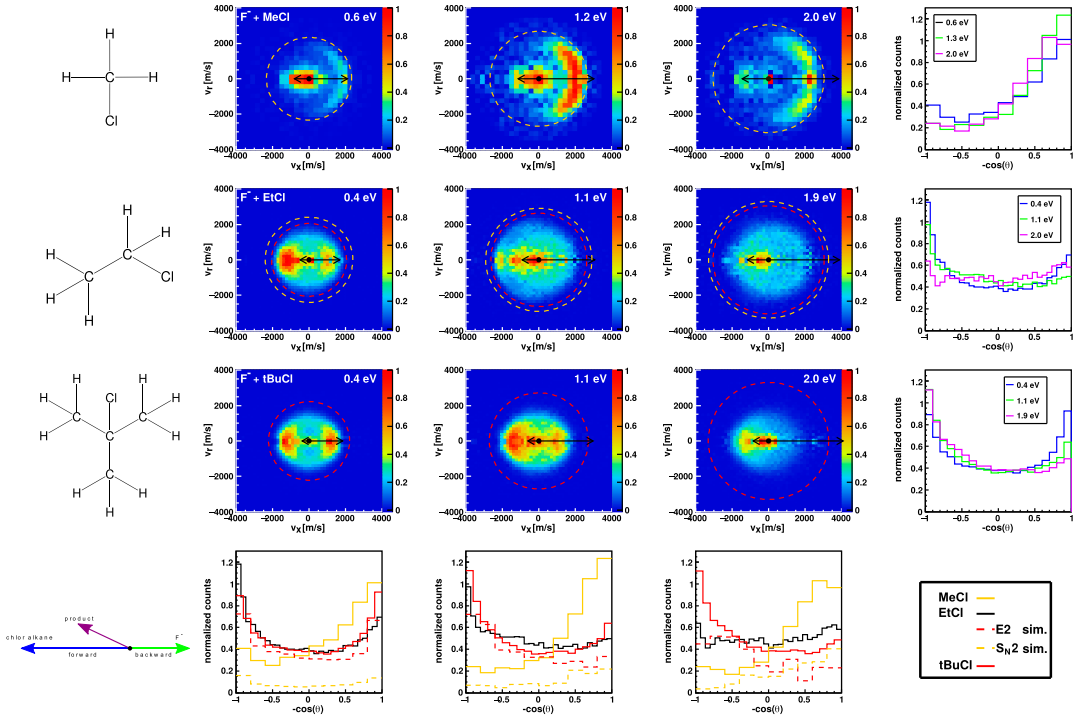

Figure 5. Product ion velocity distributions for F^- with CH_3Cl (top row), CH_3CH_2Cl (2nd row) and $(CH_3)_3CCl$ (3rd row) for three different relative collision energies ($\approx$ 0.4 eV (left column), $\approx$ 1.1 eV (2nd column) and $\approx$ 2 eV (3rd column)). The right column shows the integrated angular distribution of all three relative collision energies whereas the bottom row compares the angular distribution of the three different carbon centres. Along a column from top to bottom, the chemical complexity increases by step-wise replacing hydrogen atoms by methyl groups as substituent at the α-carbon. The rings superimposed onto the velocity distributions give the kinematic cut-offs for S_N2 (orange) and E2 (red). The same colours are used for the integrated angular distributions in (bottom row). Here, the black line gives the experimental distribution for $F^- + CH_3CH_2Cl$ while the dashed lines give the individual contributions of S_N2 (orange dashed) and E2 (red dashed) from trajectory simulations. All 1D histograms are normalised to unity. Adapted from [36].Adapted with permission from [35], copyright 2016 SpringerNature. Adapted with permission from [38], copyright 2021 SpringerNature. Adapted with permission from [37], copyright 2019 American Chemical Society.

Furthermore, it should be mentioned that both syn- and anti-elimination are energetically feasible, although syn-elimination is associated with a barrier. No trajectory simulations are yet available for reaction (10) but for $F^- + (CH_3)_3CCI$ [77]. The trajectory simulations on a full potential energy surface by Zhang *et al.* [77] could well reproduce the experimental angular and product ion kinetic energy distributions. The experimental dynamics for the larger alkyl halides are very similar for both chloride and iodide as leaving group [36,37] opposed to the methyl halides undergoing S_N2 [23,35].

The reaction between F^- and ethyl chloride is the reaction for which S_N2 and E2 are in competition with each other (Figure 5). At low relative collision energy the Cl^- velocity distribution shows a forward-backward symmetry, clearly indicating an E2 reaction. With increasing collision energy, the images show more isotropic scattering with a slight tendency towards the forward hemisphere. Scattering in the forward hemisphere in a stripping-like mechanism is a signature for direct dynamics of E2, compared to the direct-rebound mechanism of the S_N2. These seemingly dominant indirect dynamics have been shown to be misleading [38]. The experimental product ion velocity distribution is a convolution of contributions from both mechanisms and the opposing trends of S_N2 and E2 add up to an apparent isotropic signature. Quasi classical trajectory calculations [38] reveal highly direct dynamics for both mechanisms at 2 eV. The contribution of E2 is over 80% at 0.4 eV but the S_N2 fraction increases to a similar level as that of E2 at high collision energies which results in the observed isotropic velocity distribution. The presented experimental differential cross sections in synergy with high level simulations from theory allowed insights into one of the most fundamental completions of organic synthesis. Experiment and theory alike push boundaries to tackle this type of reactions [38,75,77].

4. Conclusion and outlook

The field of ion-molecule reactive scattering is rapidly advancing with new experiments and capabilities

becoming available. We are often surprised when exploring the dynamics of ion-molecule reactions because experimental results differ from our expectations which are based on our chemical or physical intuition. New experiments are set up and studies designed with two main objectives: (1) Achieving state-to-state resolution overcoming the intrinsic limitations due to working with ion beams and (2) increasing chemical complexity. These are, in our view, the areas where ion-molecule scattering will advance most within the coming years, and why we have chosen the four featured studies. The first objective is likely to focus on few-atom reactions and the second comes with increasing the number of involved atoms. While the first objective focuses more on aspects related to fundamental physics, the second focuses more on the chemistry. Both objectives push the limits of our current experimental tool-set to better understand ion molecule reactions at the most fundamental level and new experiments will push towards combining both objectives. One challenge for future experiments is set up already: Once more than two product species are formed, we lose information on the energy partitioning simply because we generally only measure a single product ion and miss out on the neutral species. Coincidence measurements will therefore be one goal to pursue to record the full kinematics of a reaction. The level of control, we exert on an ion molecule crossed beam experiments will further increase in the future as well by pushing the limits of state control with respect to polyatomic reactants or electronic states in transition metal ions. The second challenge set up is to go to lower relative collision energies. The limit is set by the ion beam whose handling at low beam velocities becomes a challenge. It will be interesting to see to which limits future experiments will be able to push down the relative collision energy in crossed beams while still having appreciable count rates. The current and coming experimental results present benchmarks for theory because the treatment of ion molecule reactions beyond the stationary points is far from trivial. Lucky for us experimentalists, theory takes up the challenge and allows the treatment of larger and more complex reactions at new levels of detail [31,38,57,67,75,77]. The article focuses on the experimental aspects but we want to stress that the synergy between experiment and theory makes a fundamental difference in understanding.

Acknowledgments

The authors are very grateful to all their co-workers. In particular, we want to thank Roland Wester without whom many of the presented studies would not have been possible and for introducing J.M. to crossed beam imaging. We also thank our collaboration partners in quantum chemistry and chemical dynamics theory, in particular Gábor Czakó, Milan Ončák and Hua Guo for the fruitful and longstanding collaborations. The authors also thank Hong Gao, Hua Guo and Roland Wester and their co-workers for providing original material, valuable discussions and feedback on the present manuscript.

Disclosure statement

No potential conflict of interest was reported by the author(s).

Funding

This work was supported by the Deutsche Forschungsgemeinschaft (DFG) under Grant 500279291. M.M. acknowledges support by the DFG through the SFB TRR88/3MET.

ORCID

Marcel Meta http://orcid.org/0009-0007-1549-9149
Jennifer Meyer http://orcid.org/0000-0003-1303-2370

References

[1] C.Y. Ng, M. Bear, I. Prigogine and S.A. Rice, editors, *State-Selected and State-to-State Ion-Molecule Reaction Dynamics*, *Adv. Chem. Phys.*, 82 Vol. Part 1 (Wiley, 1992).
[2] W.D. Geppert and M. Larsson, Chem. Rev. **113** (12), 8872–8905 (2013). doi:10.1021/cr400258m
[3] N.S. Shuman, D.E. Hunton and A.A. Viggiano, Chem. Rev. **115** (10), 4542–4570 (2015). doi:10.1021/cr5003479
[4] T.J. Millar, C. Walsh and T.A. Field, Chem. Rev. **117** (3), 1765–1795 (2017). doi:10.1021/acs.chemrev.6b00480
[5] J.M.C. Plane, W. Feng and E.C.M. Dawkins, Chem. Rev. **115** (10), 4497–4541 (2015). doi:10.1021/cr500501m
[6] R. Clausius, Ann. Phys. **176** (3), 353–380 (1857). doi:10.1002/andp.v176:3
[7] P. Langevin, Ann. Chem. Phys. **5**, 245 (1905).
[8] R.D. Levine, *Molecular Reaction Dynamics* (Cambridge University Press, Cambridge, 2009).
[9] M. Brouard and C. Vallance, editors, *Tutorials in Molecular Reaction Dynamics* (RSC Publishing, Cambridge, 2012).
[10] D.R. Herschbach, Angew. Chem. Int. Ed. **26**, 1221–1243 (1987). doi:10.1002/anie.v26:12
[11] Y. Lee, Science **236**, 793–798 (1987). doi:10.1126/science.236.4803.793
[12] J.C. Polanyi, Acc. Chem. Res. **5** (5), 161–168 (1972). doi:10.1021/ar50053a001
[13] H. Song and H. Guo, ACS Phys. Chem. Au **3** (5), 406–418 (2023). doi:10.1021/acsphyschemau.3c00009
[14] K. Höveler, J. Deiglmayr, J.A. Agner, H. Schmutz and F. Merkt, Phys. Chem. Chem. Phys. **23**, 2676–2685 (2021). doi:10.1039/D0CP06107G
[15] K. Höveler, J. Deiglmayr and F. Merkt, Mol. Phys. **119** (17-18), e1954708 (2021). doi:10.1080/00268976.2021.1954708
[16] H. Kreckel, H. Bruhns, M. Čížek, S.C.O. Glover, K.A. Miller, X. Urbain and D.W. Savin, Science **329** (5987), 69–71 (2010). doi:10.1126/science.1187191
[17] B.R. Heazlewood, Mol. Phys. **117** (14), 1934–1941 (2019). doi:10.1080/00268976.2018.1564850
[18] A. Kilaj, J. Wang, P. Straňák, M. Schwilk, U. Rivero, L. Xu, O.A. von Lilienfeld, J. Küpper and S. Willitsch, Nat.

Commun. **12** (1), 6047 (2021). doi:10.1038/s41467-021-26309-5
[19] O.A. Krohn, K.J. Catani, S.P. Sundar, J. Greenberg, G. da Silva and H.J. Lewandowski, J. Phys. Chem. A **127** (24), 5120–5128 (2023). doi:10.1021/acs.jpca.3c00914
[20] J.L. Bohn and H.J. Lewandowski, J. Phys. Chem. A **127** (38), 7869–7871 (2023). doi:10.1021/acs.jpca.3c05726
[21] E.L. Reichert and J.C. Weisshaar, J. Phys. Chem. A **106** (23), 5563–5576 (2002). doi:10.1021/jp0137827
[22] J. Mikosch, S. Trippel, C. Eichhorn, R. Otto, U. Lourderaj, J.X. Zhang, W.L. Hase, M. Weidemüller and R. Wester, Science **319** (5860), 183–186 (2008). doi:10.1126/science.1150238
[23] J. Mikosch, J. Zhang, S. Trippel, C. Eichhorn, R. Otto, R. Sun, W.A. de Jong, M. Weidemüller, W.L. Hase and R. Wester, J. Am. Chem. Soc. **135** (11), 4250–4259 (2013). doi:10.1021/ja308042v
[24] L. Pei, E. Carrascosa, N. Yang, S. Falcinelli and J.M. Farrar, J. Phys. Chem. Lett. **6** (9), 1684–1689 (2015). doi:10.1021/acs.jpclett.5b00517
[25] J. Hu, J.C. Xie, C.X. Wu and S.X. Tian, J. Chem. Phys. **154** (23), 234303 (2021). doi:10.1063/5.0055002
[26] G. Zhang, L. Guan, Z. Yan, M. Cheng and H. Gao, Chin. J. Chem. Phys. **34** (1), 71–80 (2021). doi:10.1063/1674-0068/cjcp2012219
[27] M. Meta, M.E. Huber, T. Michaelsen, A. Ayasli, M. Ončák, R. Wester and J. Meyer, J. Phys. Chem. Lett. **14** (24), 5524–5530 (2023). doi:10.1021/acs.jpclett.3c01078
[28] J. Meyer and R. Wester, Annu. Rev. Phys. Chem. **68** (1), 333–353 (2017). doi:10.1146/physchem.2017.68.issue-1
[29] E. Carrascosa, J. Meyer and R. Wester, Chem. Soc. Rev. **46** (24), 7498–7516 (2017). doi:10.1039/C7CS00623C
[30] R. Wester, Phys. Chem. Chem. Phys. **16**, 396–405 (2014). doi:10.1039/C3CP53405G
[31] G. Zhang, D. Lu, Y. Ding, L. Guan, S. Han, H. Guo and H. Gao, Nat. Chem. **15**, 1255–1261 (2023). doi:10.1038/s41557-023-01278-y
[32] M. Stei, E. Carrascosa, A. Dörfler, J. Meyer, B. Olasz, G. Czakó, A. Li, H. Guo and R. Wester, Sci. Adv. **4** (7), eaas9544 (2018). doi:10.1126/sciadv.aas9544
[33] T. Michaelsen, B. Bastian, A. Ayasli, P. Strübin, J. Meyer and R. Wester, J. Phys. Chem. Lett. **11** (11), 4331–4336 (2020). doi:10.1021/acs.jpclett.0c01095
[34] T. Michealsen, B. Bastian, P. Strübin, J. Meyer and R. Wester, Phys. Chem. Chem. Phys. **22**, 12382–12388 (2020). doi:10.1039/D0CP00727G
[35] M. Stei, E. Carrascosa, M.A. Kainz, A.H. Kelkar, J. Meyer, I. Szabó, G. Czakó and R. Wester, Nat. Chem. **8** (2), 151–156 (2016). doi:10.1038/nchem.2400
[36] E. Carrascosa, J. Meyer, J. Zhang, M. Stei, T. Michaelsen, W.L. Hase, L. Yang and R. Wester, Nat. Commun. **8** (1), 25 (2017). doi:10.1038/s41467-017-00065-x
[37] J. Meyer, E. Carrascosa, T. Michaelsen, B. Bastian, A. Li, H. Guo and R. Wester, J. Am. Chem. Soc. **141** (51), 20300–20308 (2019). doi:10.1021/jacs.9b10575
[38] J. Meyer, V. Tajti, E. Carrascosa, T. Győri, M. Stei, T. Michaelsen, B. Bastian, G. Czakó and R. Wester, Nat. Chem. **13** (10), 977–981 (2021). doi:10.1038/s41557-021-00753-8
[39] A.T.J.B. Eppink and D.H. Parker, Rev. Sci. Instrum. **68** (9), 3477–3484 (1997). doi:10.1063/1.1148310
[40] S. Trippel, M. Stei, R. Otto, P. Hlavenka, J. Mikosch, C. Eichhorn, A. Lourderaj, J. Zhang, W.L. Hase, M. Weidemüller and R. Wester, J. Phys.: Conf. Ser. **194**, 012046–012046 (2009).
[41] H. Li and A.G. Suits, Phys. Chem. Chem. Phys. **22**, 11126–11138 (2020). doi:10.1039/D0CP00522C
[42] G. Zhang, L. Guan, M. Cheng and H. Gao, Rev. Sci. Instrum. **92** (11), 113302 (2021). doi:10.1063/5.0071842
[43] D. Swaraj, T. Michaelsen, A. Khan, F. Zappa, R. Wild and R. Wester, Mol. Phys. e2194455 (2023). doi:10.1080/00268976.2023.2194455
[44] J.C. Polanyi, Science **236** (4802), 680–690 (1987). doi:10.1126/science.236.4802.680
[45] D. Schröeder, S. Shaik and H. Schwarz, Acc. Chem. Res. **33** (3), 139–145 (2000). doi:10.1021/ar990028j
[46] P. Recio, S. Alessandrini, G. Vanuzzo, G. Pannacci, A. Baggioli, D. Marchione, A. Caracciolo, V.J. Murray, P. Casavecchia, N. Balucani, C. Cavallotti, C. Puzzarini and V. Barone, Nat. Chem. **14** (12), 1405–1412 (2022). doi:10.1038/s41557-022-01047-3
[47] J.H. Futrell, in *Advances in Chemical Physics*, Vol. 82 (1992, Wiley), pp. 501–552.
[48] K. Birkinshaw, A. Shukla, S. Howard and J.H. Futrell, Chem. Phys. **113** (1), 149–158 (1987). doi:10.1016/0301-0104(87)80227-6
[49] R. Candori, S. Cavalli, F. Pirani, A. Volpi, D. Cappelletti, P. Tosi and D. Bassi, J. Chem. Phys. **115** (19), 8888–8898 (2001). doi:10.1063/1.1413980
[50] A.L. Rockwood, S.L. Howard, W.H. Du, P. Tosi, W. Lindinger and J.H. Futrell, Chem. Phys. Lett. **114** (5-6), 486–490 (1985). doi:10.1016/0009-2614(85)85126-5
[51] S.L. Howard, Chem. Phys. Lett. **178** (1), 65–68 (1991). doi:10.1016/0009-2614(91)85054-Z
[52] J. Mikosch, H. Kreckel, R. Wester, R. Plasil, J. Glosik, D. Gerlich, D. Schwalm and A. Wolf, J. Chem. Phys. **121**, 11030–11037 (2004). doi:10.1063/1.1810512
[53] S. Trippel, M. Stei, J.A. Cox and R. Wester, Phys. Rev. Lett. **110**, 163201–163201 (2013). doi:10.1103/PhysRevLett.110.163201
[54] R. Candori, F. Pirani, D. Cappelletti, P. Tosi and D. Bassi, Int. J. Mass Spectrom. **223-224**, 499–506 (2003). doi:10.1016/S1387-3806(02)00873-4
[55] J. Mikosch, U. Frühling, S. Trippel, D. Schwalm, M. Weidemüller and R. Wester, Phys. Chem. Chem. Phys. **8**, 2990–2999 (2006). doi:10.1039/B603109A
[56] Z. Hua, Y. Zhao, G. Hu, S. Feng, Q. Zhang, Y. Chen and D. Zhao, J. Phys. Chem. Lett. **12** (16), 4012–4017 (2021). doi:10.1021/acs.jpclett.1c00798
[57] B. Jiang, J. Li and H. Guo, J. Phys. Chem. Lett. **11** (13), 5120–5131 (2020). doi:10.1021/acs.jpclett.0c00989
[58] M. Besemer, G. Tang, Z. Gao, A. van der Avoird, G.C. Groenenboom, S.Y.T. van de Meerakker and T. Karman, Nat. Chem. **14** (6), 664–669 (2022). doi:10.1038/s41557-022-00907-2
[59] Z.F. Sun, M.C. van Hemert, J. Loreau, A. van der Avoird, A.G. Suits and D.H. Parker, Science **369** (6501), 307–309 (2020). doi:10.1126/science.aan2729
[60] R. Wesendrup and H. Schwarz, Angew. Chem. Int. Ed. **34** (18), 2033–2035 (1995). doi:10.1002/anie.v34:18
[61] G.K. Koyanagi and D.K. Bohme, J. Phys. Chem. A **110** (4), 1232–1241 (2006). doi:10.1021/jp0526602

[62] N. Levin, J.T. Margraf, J. Lengyel, K. Reuter, M. Tschurl and U. Heiz, Phys. Chem. Chem. Phys. **24**, 2623–2629 (2022). doi:10.1039/D1CP04469A
[63] J.G. Wang, C.J. Liu, Y.P. Zhang and B. Eliasson, Chem. Phys. Lett. **368** (3-4), 313–318 (2002). doi:10.1016/S0009-2614(02)01866-3
[64] K. Liu, Annu. Rev. Phys. Chem. **67** (1), 91–111 (2016). doi:10.1146/physchem.2016.67.issue-1
[65] K. Liu, J. Chem. Phys. **142** (8), 080901 (2015). doi:10.1063/1.4913323
[66] J. Xie, R. Otto, J. Mikosch, J. Zhang, R. Wester and W.L. Hase, Acc. Chem. Res. **47** (10), 2960–2969 (2014). doi:10.1021/ar5001764
[67] J. Xie and W.L. Hase, Science **352** (6281), 32–33 (2016). doi:10.1126/science.aaf5172
[68] R. Wester, Mass Spectrom. Rev. **41** (4), 627–644 (2022). doi:10.1002/mas.v41.4
[69] Y. Wang, H. Song, I. Szabó, G. Czakó, H. Guo and M. Yang, J. Phys. Chem. Lett. **7** (17), 3322–3327 (2016). doi:10.1021/acs.jpclett.6b01457
[70] E. Carrascosa, M. Stei, B. Bastian, J. Meyer, J. Mikosch and R. Wester, J. Phys. Chem. A **120** (27), 4711–4719 (2016). doi:10.1021/acs.jpca.5b11181
[71] H. Guo and B. Jiang, Acc. Chem. Res. **47** (12), 3679–3685 (2014). doi:10.1021/ar500350f
[72] F.A. Carey and R.J. Sundberg, *Advanced Organic Chemistry* (Springer, New York, 2007).
[73] P. Walden, Ber. Dtsch. Chem. Ges. **29**, 133–138 (1896). doi:10.1002/cber.v29:1
[74] E. Carrascosa, J. Meyer, T. Michaelsen, M. Stei and R. Wester, Chem. Sci. **9** (3), 693–701 (2018). doi:10.1039/C7SC04415A
[75] T. Gstir, T. Michaelsen, B.A. Long, A.B. Nacsa, A. Ayasli, D. Swaraj, F. Zappa, F. Trummer, S.G. Ard, N.S. Shuman, G. Czakó, A.A. Viggiano and R. Wester, Phys. Chem. Chem. Phys. **25**, 18711–18719 (2023). doi:10.1039/D3CP02110F
[76] E. Carrascosa, M. Bawart, M. Stei, F. Linden, F. Carelli, J. Meyer, W.D. Geppert, F.A. Gianturco and R. Wester, J. Chem. Phys. **143** (18), 184309–184309 (2015). doi:10.1063/1.4934993
[77] X. Lu, C. Shang, L. Li, R. Chen, B. Fu, X. Xu and D.H. Zhang, Nat. Comm. **13** (1), 4427 (2022). doi:10.1038/s41467-022-32191-6